Molecular Characterization and Localization of the NAD(P)H Oxidase Components gp91-*phox* and p22-*phox* in Endothelial Cells

Ulvi Bayraktutan, Lynda Blayney, Ajay M. Shah

Abstract—The production of reactive oxygen species (ROS) within endothelial cells may have several effects, including alterations in the activity of paracrine factors, gene expression, apoptosis, and cellular injury. Recent studies indicate that a phagocyte-type NAD(P)H oxidase is a major source of endothelial ROS. In contrast to the high-output phagocytic oxidase, the endothelial enzyme has much lower biochemical activity and a different substrate specificity (NADH>NADPH). In the present study, we (1) cloned and characterized the cDNA and predicted amino acid structures of the 2 major subunits of rat coronary microvascular endothelial cell NAD(P)H oxidase, gp91-*phox* and p22-*phox*; (2) undertook a detailed comparison with phagocytic NADPH oxidase sequences; and (3) studied the subcellular location of these subunits in endothelial cells. Although these studies revealed an overall high degree of homology (>90%) between the endothelial and phagocytic oxidase subunits, the endothelial gp91-*phox* sequence has potentially important differences in a putative NADPH-binding domain and in putative glycosylation sites. In addition, the subcellular location of the endothelial gp91-*phox* and p22-*phox* subunits is significantly different from that reported for the neutrophil oxidase, in that they are predominantly intracellular and collocated in the vicinity of the endoplasmic reticulum. This first detailed characterization of gp91-*phox* and p22-*phox* structure and location in endothelial cells provides new data that may account, in part, for the differences in function between the phagocytic and endothelial NAD(P)H oxidases. **(*Arterioscler Thromb Vasc Biol*. 2000;20:1903-1911.)**

Key Words: endothelium ■ NADPH oxidase ■ reactive oxygen species ■ cDNA

The endothelium has a vital role in the physiological regulation of vascular and cardiac muscle function. Endothelial "activation" and dysfunction are key early events in the development of atherosclerosis and other cardiovascular disorders.[1,2] It has been shown that reactive oxygen species (ROS) generated within endothelial cells or produced extracellularly may be involved in several aspects of these processes. Low-level ROS production can modulate the activity of several intracellular signaling pathways, affect the release/activity of paracrine factors, and alter gene expression.[1,3–8] Endothelial ROS may also promote apoptosis and cellular injury, eg, during ischemia/reperfusion.[9] The identification and characterization of sources of ROS within endothelial cells are therefore of interest.

Potential sources of ROS in endothelial cells include xanthine oxidase, nitric oxide synthases, NAD(P)H-dependent electron transport chains, NAD(P)H-dependent oxidoreductases, cyclooxygenase, lipoxygenase, and autooxidation of tissue metabolites.[1] Wolin and colleagues (Mohazzab et al[10]) have shown that at a biochemical level, a microsomal NADH oxidoreductase is a major source of ROS in coronary endothelial cells. Recent reports suggest that at a molecular level, this enzyme may be analogous to the neutrophil NADPH oxidase complex.[11,12] Several components similar or identical to those of the neutrophil NADPH oxidase complex have been detected in endothelial cells by reverse transcription–polymerase chain reaction (RT-PCR) and/or immunolabeling.[11,12] Indirect evidence for the presence of a functional phagocyte-type NADPH oxidase in endothelial cells also derives from studies with putative pharmacological inhibitors of the enzyme, although these inhibitors are not fully specific.[10,12,13]

The neutrophil NADPH oxidase plays a vital role in nonspecific host defense against pathogens by generating large (millimolar) quantities of superoxide during the so-called respiratory burst.[14] It comprises a membrane-associated, low-potential cytochrome (cytochrome b_{558}) and 4 or more cytosolic subunits (p47-*phox*, p67-*phox*, p40-*phox*, p21*rac*1, and Rap1A).[14–16] Cytochrome b_{558} is considered to be the most important component of the complex with respect to both enzymatic stability and activity, ie, the reduction of molecular O_2 to superoxide. Enzyme activation involves translocation of the cytosolic components to the membrane and association with the cytochrome. Cytochrome b_{558} is a

Received September 21, 1999; revision accepted April 24, 2000.

From the Departments of Cardiology, GKT School of Medicine (U.B., A.M.S.), King's College, London, and the University of Wales College of Medicine (L.B.), Cardiff, UK.

Correspondence to Professor Ajay M. Shah, Department of Cardiology, GKT School of Medicine, King's College London, Bessemer Road, London SE5 9PJ, UK. E-mail ajay.shah@kcl.ac.uk

Arterioscler Thromb Vasc Biol. **is available at http://www.atvbaha.org**

heterodimer comprising an α-subunit (p22-*phox* [for *ph*agocyte *ox*idase]) and a heavily glycosylated β-subunit (gp91-*phox*), with apparent molecular weights on SDS gels of ≈22 and 65 to 91 kDa, respectively. In resting neutrophils, the NADPH oxidase is dormant but can be rapidly activated by various receptor-dependent and -independent stimuli.

The biochemical activity of the endothelial enzyme differs substantially from that of the phagocyte NADPH oxidase.[10,12] First, the endothelial oxidase is continuously active at a low level even in nonstimulated cells. Second, it never generates a level of ROS comparable to the high burst activity of the phagocytic enzyme. Third, it appears to utilize both NADH and NADPH as substrates, but with NADH driving significantly more superoxide production than NADPH [hence the term NAD(P)H oxidase or NADH/NADPH oxidase], whereas the phagocytic oxidase preferentially utilizes NADPH. The endothelial oxidase is thus likely to subserve different functions compared with the phagocyte oxidase. The reasons for these differences are not known, mainly because of the very limited characterization of the endothelial enzyme. In vascular smooth muscle (VSM) cells, it has been shown recently that an NAD(P)H oxidase with similar biochemical properties to those of the endothelial enzyme is present and may be involved in the pathophysiology of hypertension and atherosclerosis.[17–20] One reason postulated for the different activity of the VSM enzyme compared with the phagocyte oxidase is that the gp91-*phox* subunit of cytochrome b_{558} appears to be absent and has been suggested to be expressed as a distinct isoform.[19] Indeed, a novel protein termed Mox1 (for *m*itogenic *ox*idase) with ≈56% homology to gp91-*phox* was recently reported to be expressed in VSM cells, where it is thought to be an integral component of the NAD(P)H oxidase.[21] However, in endothelial cells, both p22-*phox* and gp91-*phox* mRNA and protein were found to be expressed,[12] although a detailed analysis of these subunits has not been reported.

The aims of the present study were therefore to (1) clone and sequence the cDNAs for p22-*phox* and gp91-*phox* in rat coronary microvascular endothelial cells (CMECs), (2) undertake comparison analyses of deduced amino acid sequences between the endothelial cytochrome b_{558} subunits (present study) and published phagocytic sequences, and (3) study the intracellular location of these 2 subunits in endothelial cells.

Methods

CMEC Culture

CMECs were isolated from 12-week-old male Wistar rat hearts by retrograde collagenase digestion and differential centrifugation, according to the method of Piper et al,[22] as described previously.[12] In brief, hearts were initially perfused with the following solution (in mmol/L): NaCl 118, KCl 4.7, NaH_2PO_4 1.2, $MgSO_4$ 1.2, $NaHCO_3$ 25, and glucose 11, pH 7.4, at 37°C (gassed with 95% O_2/5% CO_2; buffer 1). Epicardial mesothelial cells were devitalized with 70% (vol/vol) ethanol. Buffer 1 with added $CaCl_2$ (0.25 mmol/L) and collagenase (0.04%, Sigma type II) was recirculated for 30 minutes. Ventricles, excluding visible large vessels, were chopped into 15 mL of recirculating solution containing BSA (200 mg, Sigma fraction V) and triturated for 10 minutes at 37°C. After filtration and centrifugation (150*g*, 3 minutes) to remove myocytes, the supernatant was incubated for 15 minutes at 37°C with added BSA (100 mg), trypsin (0.01%), and $CaCl_2$ (50 mmol/L). The CMEC pellet was obtained by centrifugation (1000*g*, 10 minutes), washed, and resuspended in 40 mL of prewarmed medium 199 (Gibco) with added 10% newborn calf serum, 10% fetal calf serum, benzylpenicillin (250 U/mL), streptomycin (250 mg/mL), amphotericin B (12.5 mg/mL), and gentamicin (50 mg/mL). Cell suspensions were plated in 75-cm^2 culture flasks and incubated at 37°C. Unattached cells and debris were washed off after 1 hour. Cultured cells formed confluent monolayers within 5 to 7 days. Cells were trypsinized and subcultured to confluence in fresh flasks. Cultured CMECs were characterized by their typical "cobblestone" morphology, uptake of fluorescently labeled acetylated LDL by >99% of cells, and the rapid formation of capillary-like tubes on the basement membrane preparation Matrigel.[12]

Reverse Transcription–Polymerase Chain Reaction

Total cellular RNA was isolated by the phenol-chloroform–guanidinium isothiocyanate method.[23] First-strand cDNA synthesis was performed by using 10 μg of total RNA with 500 ng of random hexamers (Promega), 10 mmol/L of each dNTP (Boehringer), 10 mmol/L Tris-HCl (pH 8.4), 50 mmol/L KCl, 2.5 mmol/L $MgCl_2$ and 33 U of the RNase inhibitor RNasin (Promega). Reaction mixtures were preincubated at 70°C for 3 minutes, followed by cooling on ice for 2 minutes, before addition of 200 U of Moloney murine leukemia virus reverse transcriptase (Gibco-BRL). RT was performed at 42°C for 90 minutes. PCR primers for initial amplification of p22-*phox* were based on the published rat aortic VSM sequence: sense, 5′-GACGCTTCACGCAGTGGTACT-3′; antisense, 5′-CACGACCTCATCTGTCACTGG-3′ (GenBank accession No. U18729).[24] Initial primers for amplification of gp91-*phox* were based on the published porcine phagocyte cDNA sequence (GenBank accession No. UO2476),[25] and additional primers were then designed on the basis of partial sequence data. The primers used were as follows: sense, 5′-GTCGTCATCACGCTGTGT-3′, 5′-GCCTGTGGCTGTGATAAGCAG-3′, 5′-GTGGTCATTACCAAGGTGGTC-3′, and 5′-ATGGTGGCGTGGATGATTGC-3′ (forward primers 1 to 4, respectively); antisense, 5′-CTTTTGCAGGCCTGTGA-3′, 5′-GAACATGGGACCCACGATCCA-3′, 5′-GAAAATGTATTGTCCCACCTC-3′, and 5′-TTAGAAGTTTTCCTTATTGAA-3′ (reverse primers 1 to 4, respectively). PCR was carried out in a total volume of 100 μL containing 2 μL of RT reaction, 48 ng each of sense and antisense primers, 200 mmol dNTPs, 1.5 mmol/L Mg^{2+}, and 2.5 U *Taq* polymerase (Promega). The conditions were 25 to 35 cycles of denaturation at 94°C (1 minute), annealing at 65°C (1 minute), and extension at 72°C (2 minutes), followed by a 10-minute extension reaction at 72°C. For sequence determinations, PCR was carried out by using the Advantage KlenTaq polymerase mix (ClonTech), which includes KlenTaq-1 DNA polymerase (a 5′-exo-minus, *N*-terminal deletion of *Taq* DNA polymerase), a second DNA polymerase to provide 3′→5′ proofreading activity, and TaqStart antibody to provide the automatic "hotstart" PCR.[26] At least 3 independent reactions were performed for each length of sequence.

5′-Rapid Amplification of cDNA Ends

These were performed by using the marathon RACE (rapid amplification of cDNA ends) cDNA amplification kit (ClonTech) according to the manufacturer's instructions. For amplification of 5′-untranslated regions (UTRs) of p22-*phox* and gp91-*phox*, 5′-AGTACCACTGCGTGAAGCGTC-3′ and 5′-GGCTTTGAACAGTCCCTCTGTCCAGTC-3′ gene-specific reverse primers were used, respectively. These primers were designed to have melting temperatures of at least 65°C. PolyA^+ RNA was used in first-strand cDNA synthesis, with a modified lock-docking oligo(dT) primer that contained 2 degenerate nucleotide positions at the 3′ end. RT conditions were as described above. Second-strand cDNA was synthesized by using a cocktail of *Escherichia coli* DNA polymerase I, *E coli* DNA ligase, and RNase H enzymes, which degraded the RNA before synthesis of the second-strand cDNA. Double-stranded cDNA was blunted by T4 DNA polymerase treatment before overnight ligation (16°C) of the marathon cDNA adapter, which was partially double-stranded and phosphorylated at the 5′ end to facilitate blunt-end ligation of the double-stranded cDNA by T4 DNA ligase (see the ClonTech manual for further details). After inactivation of ligase (70°C, 5 minutes), the adapter-ligated, double-stranded cDNA was diluted in Tricine-EDTA buffer before touch-

down PCR.[27] The conditions of touchdown PCR were as follows: 94°C for 1 minute; 5 cycles of 94°C for 30 seconds, 72°C for 4 minutes; 5 cycles of 94°C for 30 seconds, 70°C for 4 minutes; and finally 20 to 25 cycles of 94°C for 20 seconds, 68°C for 4 minutes.

3′-Rapid Amplification of cDNA Ends

To generate 3′-UTRs of p22-*phox* and gp91-*phox*, thermal RACE (single-sided or anchored PCR)[28] was carried out with 2 gene-specific forward primers for both p22-*phox* (No. 1, 5′-GACGCTT-CACGCAGTGGTTACT-3′; No. 2, 5′-GCAGTGGACTCCCATTG AGCC-3′) and gp91-*phox* (No. 1, 5′-GTGGTCATTACC-AAGGTGGTC-3′; No. 2, 5′-GCCTGTGGCTGTGATAAGCAG-3′). First-strand cDNA synthesis was performed with a "hybrid" primer (Q_T), consisting of oligo(dT) (17 residues) linked to a unique 18-base oligonucleotide ("adapter") primer Q_o, which in turn was linked to the second 18-base adapter primer Q_i. RT was performed under the conditions described previously. First-round PCR was performed by using the adapter primer Q_o, which binds to each cDNA at its 3′ end, and the gene-specific primers (No. 1) at moderately low annealing temperatures (54°C to 60°C). In the second-round PCR, diluted first-round PCR products were amplified with adapter primer Q_i and gene-specific primers No. 2 under more stringent conditions (annealing temperatures varied between 62°C and 67°C) to minimize generation of spurious PCR products. The sequences of the hybrid (Q_T) and adapter (Q_o and Q_i) primers were as follows: Q_T, 5′-CCAGTGAGCAGAGTGACGAGGACTCGA-GCTCAAGCTTTTTTTTTTTTTTTT-3′; Q_o, 5′-CCAGTGAGCA-GAGTGACG-3′; and Q_i, 5′-GAGGACTC GAGCTCAAGC-3′.

Sequencing Reactions

Purified PCR products were cloned into the PCR 2.1 TA cloning vector (Invitrogen) and transformed into *E coli* INVαF'-competent cells. Selected colonies were mini-prepped by alkaline lysis, and the DNA samples were sequenced on an automated ABI Prism 377 DNA sequencer (Perkin Elmer). Sequencing reactions were performed at least 3 times for each independent insert. Sequence comparisons were made with the Match-Box web server 1.2 database available on the Internet.[29]

Western Blotting

Cultured CMECs were washed twice in ice-cold PBS before lysis in 1 mL of boiling lysis solution containing 1% SDS and 10 mmol/L Tris (pH 7.4). Protein concentrations were quantified by a micro–bicinchoninic acid assay kit (Pierce). Equal amounts of protein (100 μg for p22-*phox* and 200 μg for gp91-*phox*) were run on 8% to 10% SDS polyacrylamide gels and electroblotted onto nitrocellulose membranes. Equal rates of transfer were confirmed by reversible staining with Ponceau S (Sigma). Membranes were incubated overnight at 4°C with primary antibodies, and peroxidase-conjugated secondary antibodies were used. The various anti–cytochrome b_{558} antibodies used were all originally raised against human neutrophil NADPH oxidase. Monoclonal antibodies against p22-*phox* (449) and gp91-*phox* protein (48) were provided by Dr A. Verhoeven (Amsterdam, Holland).[30] An anti–p22-*phox* rabbit polyclonal antibody (antibody α) was provided by Dr F. Wientjes (University College London, UK).[31] and an anti–gp91-*phox* rabbit polyclonal (KQS) was provided by Dr M. Quinn (Montana State University, Montana, USA).[32]

Confocal Immunofluorescence Microscopy

CMECs grown on coverslips were permeabilized and fixed with methanol (−20°C for 5 minutes).[33] Coverslips were washed and incubated with 20% fetal calf serum in PBS (pH 7.4) before incubation with different primary antibodies in PBS with 0.1% BSA and 0.01% NaN_3. Bodipy (4,4-difluoro-4-bora-3a,4a-diaza-s-indacene) fluorescein thapsigargin (Molecular Probes), which binds to the endoplasmic reticulum Ca^{2+}-ATPase, was used as a fluorescent marker for the endoplasmic reticulum and was used instead of the primary antibody at a concentration of 5 mmol/L (in 0.1% BSA in PBS, pH 7.4, at 37°C for 1 hour). These slides were washed and incubated with 0.1% BSA in PBS instead of the secondary antibody; in all other respects, these slides were subjected to the same protocol as those prepared for immunocytochemistry. For rabbit polyclonal antibodies, anti-rabbit cy3 (Amersham) was used as the secondary antibody. For mouse monoclonal antibodies, anti-mouse cy3 (Amersham) was used for single-antibody slides, and anti-mouse–FITC (Sigma) was used on dual-labeled slides. Rabbit IgG (1 μg/mL) was used instead of the primary antibody for negative controls. Two slides were prepared for each primary antibody (or combination) on each of the 3 batches of CMECs isolated, making a total of 6 slides examined for each. Confocal microscopy was performed with a Leica TCS4D microscope equipped with an argon/krypton laser.[33] The excitation wavelength was 568 nm for the cy3 conjugate and 488 nm for the FITC conjugate and bodipy FL thapsigargin. There was no overlap in fluorescence emission between these probes; ie, excitation at 568 nm elicited no significant FITC fluorescence in samples that were single-labeled with an FITC-conjugated antibody. For *x-y* sections of field size 100 mm^2 (single-labeling studies), the $\times$100 objective was used, and for 200 mm^2 (double-labeling studies), the $\times$40 objective. With a pinhole setting of 60 mm, this gave a depths of focus of $\approx$0.5 and 1 μm for the $\times$100 and $\times$40 objectives, respectively.

```
ctagaattcagcggccgctggattctcaccatggggcagatcgagtgggccatgtgggcc
                                M  G  Q  I  E  W  A  M  W  A
aacgaacaggcgctggcatctggcctgatcctcatcacagggggcatcgtggctactgcg
 N  E  Q  A  L  A  S  G  L  I  L  I  T  G  G  I  V  A  T  A
ggacgcttcacgcagtggtactttggtgcttactctattgttgcaggagtgctcatctgt
 G  R  F  T  Q  W  Y  F  G  A  Y  S  I  V  A  G  V  L  I  C
ctgctggagtacccccggggaaagaggaaaaagggctccaccatggagcggtgtggacag
 L  L  E  Y  P  R  G  K  R  K  K  G  S  T  M  E  R  C  G  Q
aagtacctgaccgctgtggtgaagctgttcgggcccctcaccagaaattactacgtccgg
 K  Y  L  T  A  V  V  K  L  F  G  P  L  T  R  N  Y  Y  V  R
gctgtcctccacttactgctgtccgtgcctgcaggcttcctgctggccaccatcctgggg
 A  V  L  H  L  L  L  S  V  P  A  G  F  L  L  A  T  I  L  G
accgtctgcttggccattgccagtgtgatctacctgctggcagccatccggggtgagcag
 T  V  C  L  A  I  A  S  V  I  Y  L  L  A  A  I  R  G  E  Q
tggactcccattgagcctaaacccaaggagcggccgcaggttggaggcaccatcaagcag
 W  T  P  I  E  P  K  P  K  E  R  P  Q  V  G  G  T  I  K  Q
ccacctaccaaccccccaccccggccaccagcggaggtccgcaagaagccaagtgaggcc
 P  P  T  N  P  P  P  R  P  P  A  E  V  R  K  K  P  S  E  A
gaagaggaggcagcctcggcaggaggaccccaggttaacccaattccagtgacagatgag
 E  E  E  A  A  S  A  G  G  P  Q  V  N  P  I  P  V  T  D  E
gtcgtgtgaccttcagtggctcctgcttgagtttccaaggtgttgctcccagagggtggt
 V  V
gatgcccactgtaataaacatggttaatagctggt
```

Figure 1. cDNA sequence and deduced amino acid sequence for rat endothelial cell p22-*phox*.

Results

Characterization of p22-*phox* cDNA in Rat Cultured CMECs

With the use of primers based on the previously published rat aortic VSM p22-*phox* cDNA sequence,[24] PCR resulted in 485-bp (expected size) products from each of several CMEC cDNA samples. A PCR product of identical size was amplified from the human monocyte–like macrophage cell line U937, which expresses cytochrome b_{558} components at high levels.[34] Negative controls performed without RT did not yield any PCR products, indicating an absence of genomic DNA contamination (data not shown). The rest of the p22-*phox* cDNA, including 5′- and 3′-UTRs, was amplified by RACE reactions. Cloning and sequencing revealed a 695-bp cDNA for rat CMEC p22-*phox*, containing an open reading frame of 579 bp and encoding 192 amino acid residues (Figure 1), with a predicted molecular weight of just under 21 kDa. A comparison of the deduced amino acid sequence of rat CMEC p22-*phox* with the previously published rat VSM sequence[24] and with several neutrophil p22-*phox* sequences[35–38] revealed a high degree of homology: 100% with the rat VSM, 87% with the human and porcine neutrophil, and 85% with the murine neutrophil sequence (Figure 2). Northern blot analysis of rat CMECs with the sequenced and cloned PCR product as a probe yielded a single band of molecular size 0.8 kb (data not shown), in

```
RAT CMEC   MGQIEWAMWANEQALASGLILITGGIVATAGRFTQWYFGAYSIVAGVLICLLEYPRGKRKKGSTMERCGQ 70
RAT VSMC   MGQIEWAMWANEQALASGLILITGGIVATAGRFTQWYFGAYSIVAGVLICLLEYPRGKRKKGSTMERCGQ
PORCINE    MGQIEWAMWANEQALASGLILMTGGIVATAGQFTQWYLGTYSIAAGVLVCLLEYPRGRRTKGSTMERCEQ
MURINE     --QIEWAMWANEQALASGLILITGGIVATAGRFTQWYFGAYSIAAGVLICLLEYPRGKRKKGSTMERCGQ
HUMAN      MGQIEWAMWANFQALASGLILITGGIVATAGRFTQWYFGAYSIVAGVFVCLLEYPRGKRKKGSTMERWGQ
BOVINE     MGQIEWAMWANEQALASGLILITGGIVATAGQFTQWYLGAYSIAAGVLVCLLEYPRGKRSKGSTMERCGQ

RAT CMEC   KYLTAVVKLFGPLTRNYYVRAVLHLLLSVPAGFLLATILGTVCLAIASVIYLLAAIRGEQWTPIEPKPKE 140
RAT VSMC   KYLTAVVKLFGPLTRNYYVRAVLHLLLSVPAGFLLATILGTVCLAIASVIYLLAAIRGEQWTPIEPKPKE
PORCINE    KYMTKVVKAFGPLSRNYYIRAFLHLGLSVPAGFLLATILGTACLAIASGIYLLAAIRGEQWTPIEPKPKE
MURINE     KYLTSVVKLFGPLTRNYYVRAALHFLLSVPAGFLLATILGTVCLAIASVIYLLAAIRGEQWTPIEPKPKE
HUMAN      KHMTAVVKLFGPFTRNYYVRAVLHLLLSVPAGFLLATILGTACLAIASGIYLLAAVRGEQWTPIEPKPRE
BOVINE     KYLTRVVKLFGPLTRNYYIRAFLHLGLAVPAGFLLATILGTACLAIASGIYLLAAIRGEQWSPIEPKPKE
                                    *
RAT CMEC   RPQVGGTIKQPPTNPPPRPPAEVRKKPSEAEEEAAS---AGGPQVNPIPVTDEVV 192
RAT VSMC   RPQVGGTIKQPPTNPPPRPPAEVRKKPSEAEEEAAS---AGGPQVNPIPVTDEVV 192
PORCINE    RPQVGGTIKQPPSNPPPRPPPEARKKPGE-E--AVAGVPRGAPRKTPCPVTDEVV 192
MURINE     RPQVGGTIKQPPTNPPPRPPAEVRKKPSEGEEEAAS---AGGPQVNPMPVTDEVV 190
HUMAN      RPQIGGTIKQPPSNPPPRPPAEARKKPSEEEAAAAAGGPPGGPQVNPIPVTDEVV 195
BOVINE     RPQIGGTIKQPPSNPPPRPPAEARKKPSE-E---AAGVPTGGPQENPMPVNDEVV 191
                      1
```

Figure 2. Comparison of predicted rat CMEC p22-*phox* peptide sequence with published rat VSM cell and various phagocyte p22-*phox* sequences. Asterisk denotes a conserved histidine residue thought to be involved in heme binding. The proline-rich region numbered 1 is thought to be involved in binding p47-*phox*. Bold letters indicate positions where the amino acid residue in 1 sequence is different from all other sequences.

agreement with the size of p22-*phox* mRNA in neutrophils of several species.[35–38]

Characterization of gp91-*phox* cDNA in Rat Cultured CMECs

Initial PCR with primers based on the previously published porcine macrophage gp91-*phox* sequence[25] resulted in a 987-bp expected-size PCR product from each of several rat CMEC cDNA samples. U937 cell cDNA was used as a positive control, and samples without RT were used as negative controls to exclude genomic cDNA contamination (not shown). The rest of the CMEC gp91-*phox* cDNA was obtained by further PCR and RACE reactions. Cloning and sequencing of the rat CMEC gp91-*phox* cDNA revealed an open reading frame of 1713 bp encoding a primary translation product of 570 amino acid residues (Figure 3), with a predicted molecular weight of 65 349 Da and a calculated isoelectric point of 8.90. Figure 4 shows the comparative deduced amino acid alignment between rat CMEC gp91-*phox* and published bovine,[38] human,[39] porcine,[25] and murine[40] neutrophil gp91-*phox* cDNA sequences, starting from the first potential initiation codon found in the sequences. There was substantial homology between the rat CMEC sequence and the neutrophil gp91-*phox* sequences (>90% at the amino acid level) but also a number of potentially significant differences (see Discussion).

The relative abundance of gp91-*phox* mRNA in CMECs appeared to be significantly less than that of p22-*phox*, because 35 cycles of amplification compared with 25 to 28 cycles for the p22-*phox* transcript were required. In keeping with this, gp91-*phox* mRNA could not be detected by Northern blotting (data not shown).

Expression and Subcellular Location of p22-*phox* and gp91-*phox* Proteins

The expression of p22-*phox* protein was confirmed by Western blotting with either a monoclonal or a polyclonal anti-neutrophil p22-*phox* antibody (449 and α, respectively), each directed against different epitopes of the protein.[30,31] Both antibodies detected an ≈22- to 23-kDa band in CMECs as well as in U937 cells (Figure 5). We have previously reported the expression of gp91-*phox* protein in rat CMECs in Western blots with the use of a monoclonal anti-neutrophil gp91-*phox* antibody (48).[12] A polyclonal anti-neutrophil gp91-*phox* antibody (KQS) directed against a different epitope of the protein[32] also detected an ≈91-kDa band in CMECs (Figure 5C). In addition, a band at ≈60 to 65 kDa was also detected, which may represent deglycosylated protein.[41] In human neutrophil membrane, the KQS antibody reacted with a broad smear from ≈55 to 100 kDa, as described previously.[14,32] This smearing pattern is thought to be due to variable glycosylation of gp91-*phox*. Of note, we did not detect a similar smearing pattern with CMEC protein with either of the anti–gp91-*phox* antibodies used.

The subcellular location of p22-*phox* and gp91-*phox* in rat CMECs was addressed by confocal immunofluorescence microscopy, using the same antibodies as reported above for

```
atggggaactgggctgtgaatgagggactctccatctttgtcattctggtgtggttgggg
 M  G  N  W  A  V  N  E  G  L  S  I  F  V  I  L  V  W  L  G
ctgaatgtcttcctctttgtcaagtattacaaggtttatgacgatgagcctaaatataat
 L  N  V  F  L  F  V  K  Y  Y  K  V  Y  D  D  E  P  K  Y  N
tacactcgaaaacttcttgggtcagcactggctctggcccgggcacctgcagcctgcctg
 Y  T  R  K  L  L  G  S  A  L  A  L  A  R  A  P  A  A  C  L
aatttcaactgcatgctgatcttgctgccagtgtgtcggaatctcctctccttcctcagg
 N  F  N  C  M  L  I  L  L  P  V  C  R  N  L  L  S  F  L  R
ggttccagtgcgtgttgctcaaccagaattcgaagacaactggacaggaaccttactttc
 G  S  S  A  C  C  S  T  R  I  R  R  Q  L  D  R  N  L  T  F
cataagatggtagcttggatgatagcacttcacacggccattcacaccattgcacatctg
 H  K  M  V  A  W  M  I  A  L  H  T  A  I  H  T  I  A  H  L
ttcaacgtggagtggtgtgtgaatgccagagtcgggacttcggacccatattcagtagca
 F  N  V  E  W  C  V  N  A  R  V  G  T  S  D  P  Y  S  V  A
ctctctaacattggagacaaagaaaatgaagagtatctcaattttgctagagaaaaaatc
 L  S  N  I  G  D  K  E  N  E  E  Y  L  N  F  A  R  E  K  I
aagaaccctgaaggggggcctgtatgtggctgtgactcggttggctggcatcacaggaatt
 K  N  P  E  G  G  L  Y  V  A  V  T  R  L  A  G  I  T  G  I
gtcatcacactgtgtcttatattgatcatcacatcctccaccaaaaccattcggaggtct
 V  I  T  L  C  L  I  L  I  I  T  S  S  T  K  T  I  R  R  S
tactttgaagtgttctggtatacacaccatctctttgtgatcttcttcatcggccttgcc
 Y  F  E  V  F  W  Y  T  H  H  L  F  V  I  F  F  I  G  L  A
atccatggagctgaacgaattgtacgtggacagacttccggacagtttgaaagagcataat
 I  H  G  A  E  R  I  V  R  G  Q  T  S  D  S  L  K  E  H  N
ttagatgtttgtgcagacaaaatcaaagaatggggaaaaataaaggagtgcccagtacca
 L  D  V  C  A  D  K  I  K  E  W  G  K  I  K  E  C  P  V  P
aagtttgccggaaaccctcctatgacttggaaatggatcgtgggtcccatgttcctgtat
 K  F  A  G  N  P  P  M  T  W  K  W  I  V  G  P  M  F  L  Y
ctgtgtgagaggctggtgcggttttggcgatctcagcagaaggtggtcattaccaaggtg
 L  C  E  R  L  V  R  F  W  R  S  Q  Q  K  V  V  I  T  K  V
gtcactcatcctttcaaaaccatcgagcttcagatgaagaagaagggattcaggatggag
 V  T  H  P  F  K  T  I  E  L  Q  M  K  K  K  G  F  R  M  E
gtgggacaatacattttcgtcaagcgtcccgcagtgtccaagctggagtggcacccctttc
 V  G  Q  Y  I  F  V  K  R  P  A  V  S  K  L  E  W  H  P  F
accctgacctctgcccctgaggaagacttctttagcatccatatccgcattgttggcgac
 T  L  T  S  A  P  E  E  D  F  F  S  I  H  I  R  I  V  G  D
tggacagagggactgttcaaagcctgtggctgtgataagcaggagtttcaagatgcctgg
 W  T  E  G  L  F  K  A  C  G  C  D  K  Q  E  F  Q  D  A  W
aaactacctaagatagcagttgatgggccctttggtacagccagtgaagatgtgttcagc
 K  L  P  K  I  A  V  D  G  P  F  G  T  A  S  E  D  V  F  S
tatgaggtggtgatgttagtgggagctgggattggagtcacgccctctgcctccattctc
 Y  E  V  V  M  L  V  G  A  G  I  G  V  T  P  S  A  S  I  L
aagtctgtctggtacaaatattgtgacaatgccaccagtctgagactcaaaaagatctac
 K  S  V  W  Y  K  Y  C  D  N  A  T  S  L  R  L  K  K  I  Y
ttctactggctgtgcagggacacgcatgcttttgagtggttcgcagacctgctgcagctc
 F  Y  W  L  C  R  D  T  H  A  F  E  W  F  A  D  L  L  Q  L
ctggagacccagatgcaagaaagaaacaatgccaacttcctcagctacaacatctacctt
 L  E  T  Q  M  Q  E  R  N  N  A  N  F  L  S  Y  N  I  Y  L
actggctgggatgaatctcaggccaatcactttgctgtgcaccacgatgaggagaaagat
 T  G  W  D  E  S  Q  A  N  H  F  A  V  H  H  D  E  E  K  D
gtgattacaggcctaaaacagaagactctgtatggacggcccaactgggataacgagttc
 V  I  T  G  L  K  Q  K  T  L  Y  G  R  P  N  W  D  N  E  F
aagaccattgcaagtcaacaccccaacaccagaataggagtttttctgtgtggccccgaa
 K  T  I  A  S  Q  H  P  N  T  R  I  G  V  F  L  C  G  P  E
gccttggctaaaactctcagtaaacagagcatctccaacttctgagtccggcccacgtgga
 A  L  A  K  T  L  S  K  Q  S  I  S  N  S  E  S  G  P  R  G
gtccacttcatcttcaacaaggaaaacttctaactcagctccgaaaaaaaggtccaaaaa
 V  H  F  I  F  N  K  E  N  F
aaaaaaaaaa
```

Figure 3. cDNA and deduced amino acid sequence for rat endothelial cell gp91-*phox*.

```
RATTUS    -MGNWAVNEGLSIFVILVWLGLNVFLFVKYYKVYDDEPKYNYTRKLLGSALALARAPAACLNFNCMLILL 69
PORCINE   ------------------------------------------------------------------
MURINE    -MGNWAVNEGLSIFVILVWLGLNVFLFINYYKVYDDGPKYNYTRKLLGSALALARAPAACLNFNCMLILL
HUMAN     -MGNWAVNEGLSIFAILVWLGLNVFLFVWYYRVYDIPPKFFYTRKLLGSALALARAPAACLNFNCMLILL
BOVINE    -MGNWVVNEGISIFVILVWLGMNVFLFVWYYRVYDIPDKFFYTRKLLGSALALARAPAACLNFNCMLILL

RATTUS    PVCRNLLSFLRGSSACCSTRIRRQLDRNLTFHKMVAWMIALHTAIHTIAHLFNVEWCVNARVGTSDPYSV 139
PORCINE   ----------------------------------MVAWMIALHATIHTIAHLFNVEWCVNARVNNSDPYSI
MURINE    PVCRNLLSFLRGSSACCSTRIRRQLDRNLTFHKMVAWMIALHTAIHTIAHLFNVEWCVNARVGISDRYSI
HUMAN     PVCRNLLSELRGSSACCSTRVRRQLDRNLTFHKMVAWMIALHSAIHTIAHLFNVEWCVNARVNNSDPYSV
BOVINE    PVCRNLLSFLRGSSACCSTRIRRQLDRNLTFHKMVAWMIALHTAIHTIAHLFNVEWCVNARVNNSDPYSI

RATTUS    ALSNIGDKENEEYLNFAREKIKNPEGGLYVAVTRLAGITGIVITLCLILIITSSTKTIRRSYFEVFWYTH 209
PORCINE   ALSDIGDKPNETYLNFVRQRIKNPEGGLYVAVTRLAGITGVVITLCLILIITSSTKTIRRSYFEVFWYTH
MURINE    ALSDIGDNENEEYLNFAREKIKNPEGGLYVAVTRLAGITGIVITLCLILIITSSTKTIRRSYFEVFWYTH
HUMAN     ALSELGDRQNESYLNFARKRIKNPEGGLYLAVTLLAGITGVVITLCLILIITSSTKTIRRSYFEVFWYTH
BOVINE    ALSDIGDKPNETYLNFVRQRIKNPEGGLYVAVTRLAGITGVVITLCLILIITSSTKTIRRSYFEVFWYTH

RATTUS    HLFVIFFIGLAIHGAERIVRGQTSDSLKEHNLDVCADKIKEWGKIKECPVPKFAGNPPMTWKWIVGPMFL 279
PORCINE   HLFVIFFIGLAIHGAERIVRRQTPKSLLVHDPKACAQNISQWGKIKDCPIPEFAGNPPMTWKWIVGPMFL
MURINE    HLFVIFFIGLAIHGAERIVRGQTAESLEEHNLDICADKIEEWGKIKECPVPKFAGNPPMTWKWIVGPMFL
HUMAN     HLFVIFFIGLAIHGAERIVRGQTAESLAVHNITVCEQKISEWGKIKECPIPQFAGNPPMTWKWIVGPMFL
BOVINE    HLFVIFFIGLAIHGAQRIVRGQTAESLLKHQPRNCYQNISQWGKIENCPIPEFSGNPPMTWKWIVGPMFL

RATTUS    YLCERLVRFWRSQQKVVITKVVTHPFKTIELQMKKKGFKMEVGQYIFVKRPAVSKLEWHPFTLTSAPEED 349
PORCINE   YLCERLVRFWRSQQKVVITKVVTHPFKTIELQMKKKGFRMEVGQYIFVKRPAVSKLEWHPFTLTSAPEED
MURINE    YLCERLVRFWRSQQKVVITKVVTHPFKTIELQMKKKGFKMEVGQYIFVKCPKVSKLEWHPFTLTSAPEED
HUMAN     YLCERLVRFWRSQQKVVITKVVTHPFKTIELQMKKKGFKMEVGQYIFVKCPKVSKLEWHPFTLTSAPEED
BOVINE    YLCERLVRFWRSQQKVVITKVVTHPFKTIELQMKKKGFKMEVGQYIFVKCPVVSKLEWHPFTLTSAPEED

RATTUS    FFSIHIRIVGDWTEGLFKACGCDKQEFQDAWKLPKIAVDGPFGTASEDVFSYEVVMLVGAGIGVTPSASI 419
PORCINE   FFSIHIRIVGDWTEGLFKACGCDKQEFQDAWKLPKIAVDGPFGTASEDVFSYQVVMLVGAGIGVTPFASI
MURINE    FFSIHIRIVGDWTEGLFNACGCDKQEFQDAWKLPKIAVDGPFGTASEDVFSYEVVMLVGAGIGVTPFASI
HUMAN     FFSIHIRIVGDWTEGLFNACGCDKQEFQDAWKLPKIAVDGPFGTASEDVFSYEVVMLVGAGIGVTPFASI
BOVINE    FFSIHIRIVGDWTEGLFKACGCDKQEFQDAWKLPKIAVDGPFGTASEDVFSYEVVMLVGAGIGVTPFASI

RATTUS    LKSVWYKYCDNATSLRLKKIYFYWLCRDTHAFEWFADLLQLLETQMQERNNANFLSYNIYLTGWDESQAN 489
PORCINE   LKSVWYKYCNNATNLRLKKIYFYWLCRDTHAFEWFADLLQLLETQMQERNNAGFLSYNIYLTGWDESQAN
MURINE    LKSVWYKYCDNATSLKLKKIYFYWLCRDTHAFEWFADLLQLLETQMQERNNANFLSYNIYLTGWDESQAN
HUMAN     LKSVWYKYCNNATNLKLKKIYFYWLCRDTHAFEWFADLLQLLESQMQERNNAGFLSYNIYLTGWDESQAN
BOVINE    LKSVWYKYCNKAPNLRLKKIYFYWLCRDTHAFEWFADLLQLLETQMQEKNNTDFLSYNICLTGWDESQAS

RATTUS    HFAVHHDEEKDVITGLKQKTLYGRPNWDNEFKTIASQHPNTRIGVFLCGPEALAKTLSKQSISNSESGPR 559
PORCINE   HFAVHHDEEKDVITGLKQKTLYGRPNWDNEFKTIASQHPTTRIGVFLCGPEALAETLNKQCISNSDSSPR
MURINE    HFAVHHDEEKDVITGLKQKTLYGRPNWDNEFKTIASEHPNTTIGVFLCGPEALAETLSKQSISNSESGPR
HUMAN     HFAVHHDEEKDVITGLKQKTLYGRPNWDNEFKTIASQHPNTRIGVFLCGPEALAETLSKQSISNSESGPR
BOVINE    HFAMHHDEEKDVITGLKQKTLYGRPNWDNEFKTIGSQHPNTRIGVFLCGPEALADTLNKQCISNSDSGPR

RATTUS    GVHFIFNKENF                                                          570
PORCINE   GVHFIFNKENF
MURINE    GVHFIFNKENF
HUMAN     GVHFIFNKENF
BOVINE    GVHFIFNKENF
```

Figure 4. Comparison of predicted rat CMEC gp91-*phox* peptide sequence with published phagocyte gp91-*phox* sequences of 4 different species. Asterisks denote conserved histidine residues considered to be involved in heme binding and coordination. Regions A and B are putative flavin-binding domains, whereas regions C through F are putative NADPH-binding domains. Region G denotes the flavin shield. Underlined motifs N-X-(S/T) marked with the symbol ∧ are potential glycosylation sites. Bold letters indicate positions where the amino acid residue in 1 sequence is different from all other sequences.

Western blotting. Figure 6A shows *x-y* confocal sections of CMECs labeled with either of the 2 anti–p22-*phox* antibodies (α and 449, respectively) or with either of the 2 anti–gp91-*phox* antibodies (KQS and 48, respectively). A consistent pattern of labeling was seen with each of the 4 antibodies: a predominantly perinuclear distribution but also a more diffuse reticular staining extending toward the cell membrane. This panel of images also shows the background controls with rabbit nonspecific IgG instead of the primary antibody. Figure 6B shows *x-y* confocal sections of CMECs dual-labeled with an anti–p22-*phox* and an anti–gp91-*phox* antibody in different combinations (1 monoclonal and 1 polyclonal). These sections demonstrated colocalization of gp91-*phox* and p22-*phox* subunits (α+48 and KQS+449, respectively). The images were entirely consistent with those of each antibody used alone (see Figure 6A). As a marker of the plasma membrane, antibody to the G-protein β-subunit (Santa Cruz) was used, and it showed a typical sarcolemma-restricted distribution and a characteristic sharp outline of these cells (Figure 6B, bottom right). The labeling pattern observed for the 2 NADPH oxidase subunits was found to be very similar to that obtained with bodipy FL thapsigargin, which binds to the endoplasmic reticulum Ca^{2+}-ATPase (Figure 6B, bottom left).

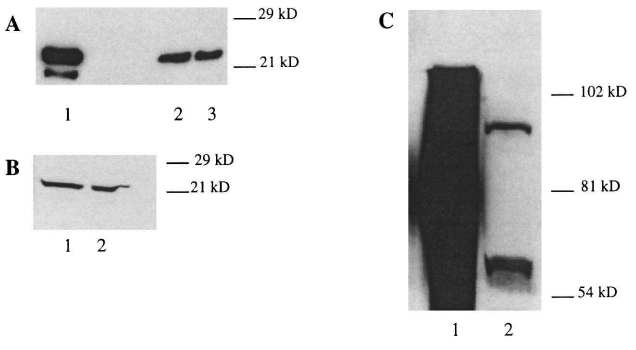

Figure 5. Western blots showing expression of p22-*phox* and gp91-*phox* protein. A, Detection of p22-*phox* with monoclonal antibody in U937 cells (lane 1), rat CMECs (lane 2), and rat VSM cells (lane 3). B, Detection of p22-*phox* with polyclonal α-antibody in U937 cells (lane 1) and rat CMECs (lane 2). C, Detection of gp91-*phox* with polyclonal KQS antibody in human neutrophil membrane (lane 1) and in rat CMECs (lane 2).

Discussion

The phagocyte NADPH oxidase is a well-characterized superoxide-generating complex that is vital for microbicidal activity.[14–16] Molecular defects in oxidase components result in chronic granulomatous disease, which is characterized by impaired or absent NADPH oxidase activity and a propensity to recurrent, life-threatening infections.[14] Recently, components of phagocyte-type NADH/NADPH oxidases have been found in several nonphagocytic cell types, including fibroblasts,[42,43] VSM cells,[19,24] coronary endothelial cells,[11,12] renal mesangial cells,[44] chemoreceptor cells,[45] microglia,[46] and bone osteoclasts.[47] In these nonphagocytic cells, it is notable that ROS production is generally of relatively low magnitude and slow kinetics compared with the burstlike millimolar production of the activated neutrophil NADPH oxidase. Potential explanations for this difference could include the possibility that oxidase subunit structures (partic-

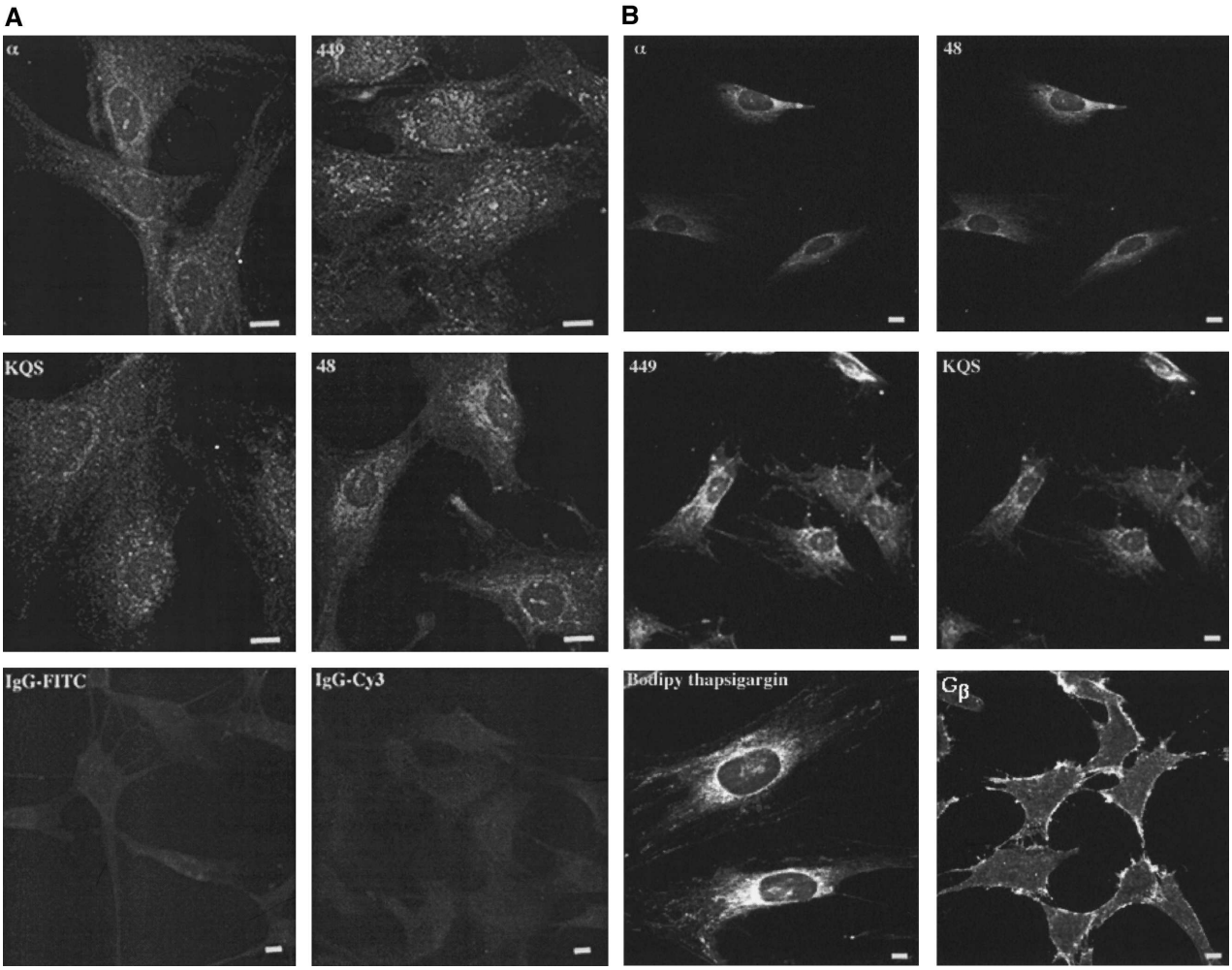

Figure 6. Subcellular localization of p22-*phox* and gp91-*phox* in rat CMECs by confocal immunofluorescence microscopy. A, Top panels show labeling with either a polyclonal or a monoclonal anti–p22-*phox* antibody (α and 449, respectively). Middle panels show labeling with either a polyclonal or a monoclonal anti–gp91-*phox* antibody (KQS and 48, respectively). Bottom panels are negative controls with nonspecific IgG. All scale bars are 10 μm. The depth of focus for this panel of pictures was 0.5 μm. B, Top panels show dual labeling with a polyclonal anti–p22-*phox* antibody and a monoclonal anti–gp91-*phox* antibody (α and 48, respectively). Middle panels show dual labeling with a monoclonal anti–p22-*phox* antibody and a polyclonal anti–gp91-*phox* antibody (449 and KQS, respectively). Bottom left panel shows labeling with a fluorescent endoplasmic reticulum marker, bodipy FL thapsigargin. Bottom right panel shows plasma membrane labeling with an anti–G_β-protein antibody. All scale bars are 10 μm. The depth of focus for this panel of pictures was 1.0 μm.

ularly that of gp91-*phox*) and/or subunit expression level, stoichiometry, and location are different among the enzymes. Indeed, in VSM, a protein with ≈56% homology to gp91-*phox,* termed Mox1, appears to substitute for gp91-*phox* in the NAD(P)H oxidase.[21]

gp91-*phox* in Rat CMECs

A detailed comparison between the deduced amino acid sequence of rat gp91-*phox* (present study) and published phagocyte gp91-*phox* sequences from several species (pig,[25] mouse,[40] human,[39] and cow[38]) indicates a high (>90%) overall degree of homology (Figure 4). For example, only 35 of 570 amino acids are different between the predicted rat CMEC sequence and the porcine macrophage gp91-*phox* sequence, which was used as the initial template for PCR amplification. Furthermore, at many of these residues, there is similarity to the phagocytic sequences of other species.

Significant information is available as to the putative functional and structural domains of phagocyte gp91-*phox*, much of it deriving from studies of patients with chronic granulomatous disease.[14–16] The histidine residues (at 101, 115, 209, and 222) located in putative transmembrane regions and potentially involved in heme binding and coordination are fully conserved among all sequences. His 115 has been suggested to be important for the H^+ channel function of gp91-*phox*.[48] His 338, which is also conserved in the endothelial sequence, is suggested to be a critical residue for FAD incorporation and thus, enzyme activity.[49] The 2 potential flavin-binding domains (A and B in Figure 4) are both fully conserved. The gp91-*phox* molecule has 4 putative NADPH-binding domains (labeled C through F in Figure 4), based on homology to ferrodoxin $NADP^+$ reductase and other related flavoproteins.[14,15] Although domains D through F are fully conserved, a striking difference occurs at residue 416 in domain C in the rat CMEC sequence, where serine is substituted for the phenylalanine present in all of the phagocyte sequences. Interestingly, a missense mutation resulting in substitution of histidine for proline has been reported at

residue 415 in chronic granulomatous disease patients, which results in decreased binding of NADPH to the oxidase and significantly reduced neutrophil O_2^- production.[50] The nonconservative substitution at residue 416 in the rat CMEC sequence could therefore also be potentially functionally important, with respect to both enzyme activity and substrate specificity. Another notable difference between the rat CMEC sequence and the phagocyte sequences is in potential glycosylation sites, which are encoded by the consensus motif N-X-(S/T), where X is any residue. The deduced rat CMEC sequence contains 3 potential glycosylation sites, namely residues 40 to 42, 97 to 99, and 430 to 432 (Figure 4). In contrast, the murine phagocyte sequence contains 4 potential glycosylation sites, and the human and bovine contain 5 each. (The porcine phagocyte sequence shown in Figure 4 has 4 potential glycosylation sites, but this sequence is considered to be incomplete.) For human neutrophil gp91-*phox*, it was suggested that the actual targets for glycosylation are residues 132 to 134, 149 to 151, and 240 to 242.[41] None of these 3 regions are consensus glycosylation motifs in the rat CMEC sequence. This difference could account for the finding that rat CMEC gp91-*phox* migrates as discrete, ≈91- and ≈60- to 65-kDa bands, whereas the phagocytic proteins generally migrate as a broad smear from ≈55 to 100 kDa. Because glycosylation may influence protein assembly, subcellular location, intracellular transport, and stability,[51] this difference may also account for the intracellular location of rat CMEC gp91-*phox* in the vicinity of the endoplasmic reticulum (Figures 6A and 6B). The putative p47-*phox*–binding domains of gp91-*phox* (residues 87 to 94, 451 to 458, 494 to 498, and 559 to 565) are all conserved in the rat CMEC sequence. It remains feasible that differences in regions of the protein to which no functional activities have been so far assigned might be important.

p22-*phox* in Rat CMECs

The coding region and 3′-UTR of the rat CMEC p22-*phox* cDNA sequence determined in the present study show 100% homology to the previously published rat VSM sequence.[24] Comparison of the rat CMEC p22-*phox* predicted amino acid sequence with those of published neutrophil sequences from several species (pig,[37] mouse,[36] human,[35] and cow[38]) reveals considerable (>90%) homology (Figure 2). It is notable that the histidine residue (His 94) suggested to be a potential heme-binding site is conserved in all sequences. Proline-rich SH_3-binding regions in the carboxy terminus of p22-*phox* (in particular, residues 151 to 160), which are suggested to be involved in binding SH_3 domains in p47-*phox*, are also highly conserved in all sequences. None of the differences between the rat CMEC/VSM p22-*phox* sequence and published neutrophil sequences suggests a significant difference between the proteins.

Protein Expression and Subcellular Location of p22-*phox* and gp91-*phox*

The expression of the 2 cytochrome b_{558} subunits at the protein level was also confirmed in CMECs. In the case of gp91-*phox*, the pattern of labeling on Western blots was different from the neutrophil pattern, as discussed above. With respect to subcellular location, a consistent labeling pattern was obtained with all of the anti–gp91-*phox* and p22-*phox* antibodies used in CMECs. Notably, the majority of labeling was clearly intracellular and appeared to be in the vicinity of the endoplasmic reticulum, as judged by the similar staining pattern observed with an endoplasmic reticulum marker. The validity of this result was reinforced by the fact that dual labeling, either with 2 anti–gp91-*phox* or 2 anti–p22-*phox* antibodies, or with a combination of 1 each, always resulted in colocalization. In neutrophils, previous studies with electron microscopy and immunogold labeling demonstrated that cytochrome b_{558} is localized mainly in granulocytes, which may fuse with the plasma membrane when neutrophils are activated.[52] A similar study with anti–gp91-*phox* antibody to label "unroofed" neutrophils, with the cytoplasmic face of the plasma membrane exposed, showed NAD(P)H oxidase subunits to be clustered in microdomains of the plasma membrane.[31] Our results suggest that in CMECs the location of NAD(P)H complex is significantly different, with most of the enzyme being clearly located intracellularly. Given the high overall homology in structure and putative transmembrane domains between the endothelial gp91-*phox* sequence and published phagocyte sequences, it seems likely that the cytochrome b_{558} subunits in endothelial cells are bound to intracellular membranes. However, the resolution of fluorescent confocal microscopy used in the present study is insufficient to establish whether the NAD(P)H oxidase subunits are indeed attached to the endoplasmic reticulum or possibly, in granules associated with it. Confirmation of the precise intracellular location would probably require electron microscopy and immunogold labeling studies.

Conclusions

An analysis of cDNA and predicted amino acid sequences of the 2 major components of NAD(P)H oxidase, p22-*phox* and gp91-*phox*, and their subcellular location in rat CMECs has been undertaken in the present study. Determination of the full rat CMEC gp91-*phox* cDNA sequence represents the first analysis of a gp91-*phox* sequence in a nonphagocytic cell type. The results indicate a number of structural differences (notably in putative NADPH binding and in glycosylation sites) that could contribute to the low but sustained biochemical activity of the endothelial oxidase. In addition, the subcellular location of the endothelial oxidase differs from that reported for the neutrophil enzyme, perhaps reflecting a different function. However, it remains feasible that factors such as the availability of heme and other cofactors,[53] a low expression level of other subunits,[54] or a defective activation process[55] could also contribute to the biochemical differences between the endothelial and phagocyte enzymes. Determination of the cDNA structure of the α- and β-subunits of endothelial NAD(P)H oxidase paves the way for further investigation of structure-function relations of this complex enzyme system.

Acknowledgments

This work was supported by the British Heart Foundation (BHF) and the Medical Research Council. A.M.S. holds the BHF Chair of Cardiology in King's College, London.

References

1. Harrison DG. Cellular and molecular mechanisms of endothelial cell dysfunction. *J Clin Invest.* 1997;100:2153–2157.

2. Ross R. Atherosclerosis: an inflammatory disease. *N Engl J Med*. 1999; 340:115–126.
3. Ohara Y, Peterson TE, Harrison DG. Hypercholesterolemia increases endothelial superoxide anion production. *J Clin Invest*. 1993;91: 2546–2551.
4. Marui N, Offermann MK, Swerlick R, Kunsch C, Rosen CA, Ahmad M, Alexander RW, Medford RM. Vascular cell adhesion molecule-1 (VCAM-1) gene transcription and expression are regulated through an antioxidant-sensitive mechanism in human vascular endothelial cells. *J Clin Invest*. 1993;92:1866–1874.
5. Cheng JJ, Chao YJ, Wung BS, Wang DL. Cyclic-strain-induced plasminogen activator inhibitor-1 (PAI-1) release from endothelial cells involves reactive oxygen species. *Biochem Biophys Res Commun*. 1996;225: 100–105.
6. Hishikawa K, Luscher TF. Pulsatile stretch stimulates superoxide production in human aortic endothelial cells. *Circulation*. 1997;96: 3610–3616.
7. Wung BS, Cheng JJ, Hsieh HJ, Shyy YJ, Wang DL. Cyclic strain–induced monocyte chemotactic protein-1 gene expression in endothelial cells involves reactive oxygen species activation of activator protein 1. *Circ Res*. 1997;81:1–7.
8. Wung BS, Cheng JJ, Chao YJ, Hsieh HJ, Wang DL. Modulation of Ras/Raf/extracellular signal–regulated kinase pathway by reactive oxygen species is involved in cyclic strain–induced early growth response-1 gene expression in endothelial cells. *Circ Res*. 1999;84: 804–812.
9. McCord JM. Oxygen-derived free radicals in post-ischemic injury. *N Engl J Med*. 1985;312:159–163.
10. Mohazzab-H KM, Kaminski PM, Wolin MS. NADH oxidoreductase is a major source of superoxide anion in bovine coronary artery endothelium. *Am J Physiol*. 1994;266:H2568–H2572.
11. Jones SA, O'Donnell VB, Wood JD, Broughton JP, Hughes EJ, Jones OTG. Expression of phagocyte NADPH oxidase components in human endothelial cells. *Am J Physiol*. 1996;271:H1626–H1634.
12. Bayraktutan U, Draper N, Lang D, Shah AM. Expression of a functional neutrophil-type NADPH oxidase in cultured rat coronary microvascular endothelial cells. *Cardiovasc Res*. 1998;38:256–262.
13. Suzuki Y, Wang W, Vu TH, Raffin TA. Effect of NADPH oxidase inhibition on endothelial cell ELAM-I mRNA expression. *Biochem Biophys Res Commun*. 1992;184:1339–1343.
14. Thrasher AJ, Keep NH, Wientjes F, Segal AW. Chronic granulomatous disease. *Biochim Biophys Acta*. 1994;1227:1–24.
15. Leusen JHW, Verhoeven AJ, Roos D. Interactions between the components of the human NADPH oxidase: intrigues in the *phox* family. *Lab Clin Med*. 1996;128:461–476.
16. DeLeo FR, Quinn MT. Assembly of the phagocyte NADPH oxidase: molecular interaction of oxidase proteins. *J Leukoc Biol*. 1996;60: 677–691.
17. Griendling KK, Minieri CA, Ollerenshaw JD, Alexander RW. Angiotensin II stimulates NADH and NADPH oxidase activity in cultured vascular smooth muscle cells. *Circ Res*. 1994;74:1141–1148.
18. Rajagopalan S, Kurz S, Munzel T, Tarpey M, Freeman BA, Griendling KK, Harrison DG. Angiotensin II-mediated hypertension in the rat increases vascular superoxide production via membrane NADH/NADPH oxidase activation. *J Clin Invest*. 1996;97:1916–1923.
19. Ushio-Fukai M, Zafari AM, Fukui T, Ishizaka N, Griendling KK. $p22^{phox}$ is a critical component of the superoxide-generating NADH/NADPH oxidase system and regulates angiotensin II-induced hypertrophy in vascular smooth muscle cells. *J Biol Chem*. 1996;271:23317–23321.
20. Mohazzab-H KM, Wolin MS. Properties of a superoxide anion-generating microsomal NADH oxidoreductase, a potential pulmonary artery PO_2 sensor. *Am J Physiol*. 1994;267:L823–L831.
21. Suh Y-A, Arnold RS, Lassegue B, Shi J, Xu X, Sorescu D, Chung AB, Griendling KK, Lambeth JD. Cell transformation by the superoxide-generating oxidase Mox1. *Nature*. 1999;401:79–82.
22. Piper HM, Spahr R, Mertens S, Krutzfeldt A, Watanabe H. Microvascular endothelial cells from heart. In: Piper HM, ed. *Cell Culture Techniques in Heart and Vessel Research*. Berlin, Germany: Springer-Verlag; 1990: 158–177.
23. Maniatis T, Fritsch EF, Sambrook J. *Molecular Cloning: A Laboratory Manual*. Cold Spring Harbor, NY: Cold Spring Harbor Laboratory Press; 1989.
24. Fukui T, Lassague B, Kai H, Alexander RW, Griendling KK. Cytochrome b-558 α-subunit cloning and expression in rat aortic smooth muscle cells. *Biochim Biophys Acta*. 1995;1231:215–219.
25. Zhou Y, Lin G, Murtaugh MP. Interleukin-4 suppresses the expression of macrophage NADPH oxidase heavy chain subunit (gp91*phox*). *Biochim Biophys Acta*. 1995;1265:40–48.
26. Kellogg DE, Rybalkin I, Chen SM, Mukhamedova N, Vlasik T, Siebert P, Chenchik A. TaqStart antibody: hotstart PCR facilitated by a neutralising monoclonal antibody directed against Taq DNA polymerase. *Biotechniques*. 1994;16:1134–1137.
27. Frohman MA. Rapid amplification of complementary DNA ends for generation of full-length complementary DNAs: thermal RACE. *Methods Enzymol*. 1993;218:340–356.
28. Don RH, Cox PT, Wainwright BJ, Baker K, Mattick JS. Touchdown PCR to circumvent spurious priming during gene amplification. *Nucleic Acids Res*. 1991;19:4008.
29. Depiereux E, Baudoux G, Briffeuil P, Reginster I, De Bolle X, Vinals C, Feytmans E. Match-Box-server: a multiple sequence alignment tool placing emphasis on reliability. *Comput Appl Biosci*. 1997;13: 249–256.
30. Verhoeven AJ, Bolscher GJM, Meerhof LJ, Zweiten R, Keijer J, Weening RS, Roos D. Characterisation of two monoclonal antibodies against cytochrome b558 of human neutrophils. *Blood*. 1989;6:1686–1694.
31. Wientjes F, Segal A, Hartwig J. Immunoelectron microscopy shows a clustered distribution of NADPH oxidase components in the human neutrophil plasma membrane. *J Leukoc Biol*. 1997;61:303–312.
32. Quinn MT, Parkos C, Walker L, Orkin S, Dinauer M, Jesaitis A. Association of Ras-related protein with cytochrome b of human neutrophils. *Nature*. 1989;342:199–200.
33. Blayney L, Gapper P, Rix C. Identification of phospholipase C β isoforms and their location in cultured vascular smooth muscle cells of pig, human and rat. *Cardiovasc Res*. 1998;40:564–572.
34. Obermeier H, Sellmayer A, Danesch U, Aepfelbacher M. Cooperative effects of interferon-γ on the induction of NADPH oxidase by retinoic acid or 1,25(OH_2)-vitamin D3 in monocytic U937 cells. *Biochim Biophys Acta*. 1995;1269:25–31.
35. Parkos CA, Dinauer MC, Walker LE, Allen RA, Jesaitis AJ, Orkin SH. Primary structure and unique expression of the 22-kilodalton light chain of human neutrophil cytochrome b. *Proc Natl Acad Sci U S A*. 1988;85: 3319–3323.
36. Sumimoto H, Nozaki M, Sasaki H, Takeshige K, Sakaki Y, Minakami S. Complementary DNA for the mouse homolog of the small subunit of human cyb558. *Biochem Biophys Res Commun*. 1989;165:902–906.
37. Zhou Y, Murtaugh MP. Cloning and expression of the gene encoding porcine NADPH oxidase light-chain subunit. *Gene*. 1994;148: 363–367.
38. Davis AR, Mascolo PL, Bunger PL, Sipes KM, Quinn MT. Cloning and sequencing of the bovine flavocytochrome b subunit proteins, gp91-*phox* and p22-*phox*: comparison with other known flavocytochrome b sequences. *J Leukoc Biol*. 1998;64:114–123.
39. Teahan C, Rowe P, Parker P, Totty N, Segal AW. The X-linked CGD gene codes for the β-chain of cyb245. *Nature*. 1987;327:720–721.
40. Bjorgvinsdottir H, Zhen L, Dinauer MC. Cloning of murine gp91*phox* cDNA and functional expression in a human X-linked chronic granulomatous disease cell line. *Blood*. 1996;5:2005–2010.
41. Wallach TM, Segal AW. Analysis of glycosylation sites on gp91*phox*, the flavocytochrome of the NADPH oxidase, by site-directed mutagenesis and translation in vitro. *Biochem J*. 1997;321:583–585.
42. Meier B, Jesaitis AJ, Emmendorffer A, Roesler J, Quinn MT. The cytochrome *b*-558 molecules involved in the fibroblast and polymorphonuclear leucocyte superoxide-generating NADPH oxidase systems are structurally and genetically distinct. *Biochem J*. 1993;289: 481–486.
43. Pagano PJ, Clark JK, Cifuentes-Pagano ME, Clark SM, Callis GM, Quinn MT. Localization of a constitutively active, phagocyte-like NADPH oxidase in rabbit aortic adventitia: enhancement by angiotensin II. *Proc Natl Acad Sci U S A*. 1997;94:14483–14488.
44. Radeke HH, Cross AR, Hancock JT, Jones OTG, Nakamura M, Kaever V, Resch K. Functional expression of NADPH oxidase components (α- and β-subunits of cytochrome b558 and 45-kDa flavoprotein) by intrinsic human glomerular mesangial cells. *J Biol Chem*. 1991;266:21025–21029.
45. Cross AR, Henderson L, Jones OTG, Delpiano MA, Hentschel J, Acker H. Involvement of an NAD(P)H oxidase as a PO_2 sensor protein in the rat carotid body. *Biochem J*. 1991;272:743–747.
46. Sankarapandi S, Zweier JL, Mukherjee G, Quinn MT, Huso DL. Measurement and characterisation of superoxide generation in microglial

cells: evidence for an NADPH oxidase-dependent pathway. *Arch Biochem Biophys*. 1998;353:312–321.
47. Moulton PJ, Goldring MB, Hancock JT. NADPH oxidase of chondrocytes contains an isoform of the gp91*phox* subunit. *Biochem J*. 1998;329:449–451.
48. Henderson LM. Role of histidines identified by mutagenesis in the NADPH oxidase-associated H^+ channel. *J Biol Chem*. 1998;273:33216–33223.
49. Yoshida LS, Saruta F, Yoshikawa K, Tatsuzawa O, Tsunawaki S. Mutation at histidine 338 of $gp91^{phox}$ depletes FAD and affects expression of cytochrome b_{558} of the human NADPH oxidase. *J Biol Chem*. 1998; 273:27879–27886.
50. Segal AW, West I, Wientjes F, Nugent JH, Chavan AJ, Haley B, Garcia RC, Rosen H, Scrace G. Cytochrome b_{-245} is a flavocytochrome containing FAD and the NADPH-binding site of the microbicidal oxidase of phagocytes. *Biochem J*. 1992;284:781–788.
51. Ruddon RW, Bedows E. Assisted protein folding. *J Biol Chem*. 1997; 272:3125–3128.
52. Jesaitis AJ, Buescher ES, Harrison D, Quinn MT, Parkos CA, Livesey S, Linner J. Ultrastructural localisation of cytochrome b in the membranes of resting and phagocytosing human granulocytes. *J Clin Invest*. 1990;85: 821–835.
53. Yu L, Zhen L, Dinauer MC. Biosynthesis of the phagocyte NADPH oxidase cytochrome b_{558}: role of heme incorporation and heterodimer formation in maturation and stability of $gp91^{phox}$ and $p22^{phox}$ subunits. *J Biol Chem*. 1997;272:27288–27294.
54. Dusi S, Nadalini KA, Donini M, Zentilin L, Wientjes FB, Roos D, Giacca M, Rossi F. Nicotinamide-adenine dinucleotide phosphate oxidase assembly and activation in EBV-transformed B lymphoblastoid cell lines of normal and chronic granulomatous disease patients. *J Immunol*. 1998; 161:4968–4974.
55. Batot G, Paclet M-H, Doussiere J, Vergnaud S, Martel C, Vignais PV, Morel F. Biochemical and immunochemical properties of B lymphocyte cytochrome. b_{558}. *Biochim Biophys Acta*. 1998;1406:188–202.